Chemical Engineering Science 271 (2023) 118545

Contents lists available at ScienceDirect

Chemical Engineering Science

journal homepage: www.elsevier.com/locate/ces

Power, mixing and flow dynamics of the novel Allegro™ stirred tank reactor

J.N. Delbridge [a], T.A. Barrett [b], A. Ducci [c], M. Micheletti [a,*]

[a] Department of Biochemical Engineering, University College London, Torrington Place, London WC1E 7JE, United Kingdom
[b] Pall Corporation, Southampton Road, Portsmouth PO6 4BQ, United Kingdom
[c] Department of Mechanical Engineering, University College London, Torrington Place, London WC1E 7JE, United Kingdom

HIGHLIGHTS

- Allegro STR 50–2000 L bioreactor range is successfully scaled down to 1 L.
- Agreement of power and mixing number across 1 to 200 L bioreactor scale.
- Square cross-section of vessel increases impeller power number.
- Mean flow characterisation of unique vessel geometry.
- Allegro STR geometry enhances mixing and kinetic energy distribution.

ARTICLE INFO

Article history:
Received 8 November 2022
Received in revised form 1 February 2023
Accepted 4 February 2023
Available online 9 February 2023

Keywords:
Elephant Ear impeller
Mixing
Single-use
Scale-down
Asymmetric vessel
Irregular baffle

ABSTRACT

The development of new biopharmaceuticals relies on robust scale-up from small-scale screening studies to industrial bioreactors. Novel SUB designs can prove highly beneficial, although they lack the extensive characterisation of traditional STRs. Pall Corporation's Allegro™ STR 50–2000 L bioreactor range has a unique design of square cross-section, with three wedge-shaped baffles. A scale-down 1 L prototype (abbreviated A-STR) was developed for characterisation studies and compared to a standard cylindrical STR (abbreviated S-STR). Agreement of power and mixing number data with that of the Allegro STR 200 L indicated successful scale-down. In down-pumping mode, mixing times in the A-STR were approximately 53 % lower than in the S-STR. However, in up-pumping mode both configurations exhibited similar mixing times. This study utilises a scale-down prototype to provide quantitative data on the commercial Allegro STR bioreactor range, to define operating parameters for enhanced scalability, and for comparison with a standard bioreactor geometry.

1. Introduction

Biopharmaceuticals (or biologics) continue to dominate the global pharmaceutical market, with eight of the top ten bestselling drugs in 2018 falling into this category (Lu et al., 2020). This class of therapeutics has a wide range of modalities including monoclonal antibodies (mAbs), recombinant proteins, enzymes, vaccines, and cell and gene therapies to name a few (Narayanan, Sponchioni and Morbidelli, 2022). Crucial to the success of developing new therapeutics is the early screening of protein producing cell lines for high productivity, in addition to optimising culture conditions such as media composition, pH and dO_2 levels, feeding techniques, agitation and gassing strategies (Nienow et al., 2013). However, despite extensive screening and selection of operating parameters, candidates found to be productive at small-scale run the risk of poor performance in industrial scale stirred tank reactors (STRs). While impeller induced shear has often been indicated as the main factor for this lack of scalability, a number of studies have shown otherwise, with shear damage mainly caused by bubble burst in the absence of surfactants (Godoy-Silva et al., 2009a; Nienow, 2021). The trade-off between mixing time and shear damage often results in the operation of bioreactors at below optimal agitation rates due to the overestimation of animal cell shear sensitivity (Godoy-Silva et al., 2009a; Godoy-Silva et al., 2009b; Nienow et al., 2013). This issue becomes more problematic with

Abbreviations: SUB, single use bioreactor; A-STR, Allegro stirred tank reactor; UP, up-pumping; DP, down-pumping.

* Corresponding author.
E-mail address: m.micheletti@ucl.ac.uk (M. Micheletti).

https://doi.org/10.1016/j.ces.2023.118545
0009-2509/

Nomenclature

Roman characters

B_W	baffle width, m
C	impeller clearance from tank bottom to mid-impeller, m
D	impeller diameter, m
F	force exerted on gauge due to impeller motion, N
H	bioreactor height, m
H_L	liquid height, m
r, z, w	axial, radial, and tangential components
k	time resolved turbulent kinetic energy due to turbulence and blade passage, m2/s^{-2}(−|-)
l	lever arm, m
M	percentage of mixed pixels, %
N	impeller rotational speed, s^{-1}
n	number of experimental repeats, dimensionless
N_P	impeller power number, dimensionless
P	power input, W
P_o	power number
Q	fluid volumetric flow rate, m^3/s
t_m	mixing time, s
T	vessel internal diameter, m
T_q	impeller torque, N m
u'	ensemble-averaged standard deviations of the respective velocity components
r	radial distance, m
Re	Reynolds number, dimensionless
U_r,U_z,U_w	radial, axial, and tangential components of instantaneous velocity, m/s
$\bar{U}_r$, $\bar{U}_z$,$\bar{U}_w$,	ensemble averaged magnitude of radial, axial, and tangential velocity, m/s
$\bar{U}_{rz}$	ensemble-averaged magnitude of radial and axial velocity components, m/s
V_{tip}	impeller tip velocity, ms^{-1}
V_L	liquid volume, L
W	impeller height

Greek characters

Θ	tangential direction angle, deg
λ	wavelength, nm
μ	dynamic viscosity, kg m^{-1} s^{-1}
ν	kinematic viscosity, m^2/s
ρ_L	fluid density, kg m^{-3}
σ_G	standard deviation of green pixel intensity, [-]

Abbreviations

2D	two dimensional
3D	three dimensional
A-STR	Allegro STR bioreactor 1 L prototype
CIP	clean-in-place
CFD	computational fluid dynamics
CHO	Chinese hamster ovary
CQA	critical quality attribute
DP	down-pumping
EDR	energy dissipation rate
EE	Elephant Ear impeller
HE-3	Chemineer high efficiency impeller
LDA	laser Doppler anemometry
LED	light emitting diode
MAb	monoclonal antibody
MR	methyl red
PIV	particle image velocimetry
rpm	revolutions per minute
SLA	stereolithography
STR	stirred tank reactor
S-STR	standard stirred tank reactor configuration
SUB	single-use bioreactor
TB	thymol blue
UP	up-pumping
vvm	volume of air per volume of culture per minute

scale-up, where an inherent increase in mixing time causes more prominent heterogeneities. Although animal cell cultures do not have as extensive oxygen requirements as microbial cultures, adequate mixing is required to avoid spatial gradients in pH, temperature, dissolved oxygen, CO_2 partial pressure, or substrate concentration (Nienow et al., 2013; Paul and Herwig, 2020). Such gradients have been shown to impact viable cell density, productivity, and product critical quality attributes (CQAs) such as mAbs glycosylation patterns (Chotigeat et al., 1994; Osman, Birch and Varley, 2002; Restelli et al., 2006). Temporal homogeneity in stirred tanks was found to be particularly problematic with pH gradients at the surface of the culture medium, where base is typically added for pH control (Nienow et al., 2013). Increases in pH of as much as 0.8 units have been recorded due to alkali addition at the medium surface (Langheinrich and Nienow, 1999), while a scale-down study has found that such inhomogeneity greatly reduced viable cell density when growing GS-NS0 mouse myeloma cells (Nienow et al., 2013).

To account for the heterogeneities experienced by cells cultured in industry scale STRs, key process development is usually carried out in 1–30 L STRs. In an effort to reduce the discrepancies between screening in shake flasks and production in industry scale STRs, microscale parallel stirred bioreactors have also been developed (Hsu et al., 2012; Velez-Suberbie et al., 2018; Sewell et al., 2019; Teworte et al., 2022). However, microscale bioreactors generally operate at lower Reynolds numbers without the turbulent flow conditions found in industrial STRs (Nienow et al., 2013; Tajsoleiman et al., 2019). A study by Nienow *et al.* (2013) on the much-debated topic of shear sensitivity concluded that cell shear thresholds are best studied in turbulent bench-scale STRS, however, shear due to impeller agitation at typical power input (10–150 W/m^3) is highly unlikely to damage entities as robust as CHO (Chinese hamster ovary) cells. Nevertheless, it remains that shear may be the root cause of failure with scale-up in processes with greater sensitivity to shear, such as transient transfection (Chen et al., 2019). Therefore, from a process development point of view, it is beneficial to reproduce the flow conditions encountered in industrial STRs in scale-down systems.

In addition to optimisation of process conditions, costs of biopharmaceuticals manufacturing can be further reduced by the adoption of single-use bioreactors (SUBs) over their traditional stainless steel counterparts. SUBs are beneficial in their reduction of capital costs, contamination risks, down-time and energy expenditure by elimination of CIP (clean-in-place) procedures, and by providing greater process flexibility in manufacturing plants (Lopes, 2015). Pall Corporation's Allegro™ STR is one such SUB range, which was notably used to achieve low costs and consistent product quality across the scale in the rapid development of the ChAdOx1 nCoV-19 vaccine (Joe et al., 2022). Although the typical cylindrical dished head tank seen in stainless-steel systems has been the tried and tested method of large scale cell culture for decades of industry operations, the growth of the single-use bioreactor

market has brought with it the opportunity for novel designs. These designs are often adapted in light of process considerations and practicality requirements. Previous characterisation studies in literature are mostly based on standard stirred tank geometries rather than those of commercial bioreactors (Samaras, Ducci and Micheletti, 2020). Extensive characterisation of such novel designs is beneficial in establishing reliable process parameters and robust scaling procedures. The Allegro STR bioreactor range, agitated by a low shear Elephant Ear (EE) impeller, is particularly unique in its biocontainer geometry. While the biocontainer itself is cubical, the surrounding support structure creates rounded edges and forms three large asymmetrically placed wedge-shaped baffles.

A study on the Ambr® 15 determined that the rectangular cross-section acts as a form of baffling, improving blending by preventing swirling flow that typically occurs in unbaffled STRs of circular cross-section (Nienow et al., 2013). The HyPerforma™ DynaDrive™ is another newly designed SUB utilising a cuboid vessel to improve mixing performance (Samaras, Micheletti and Ding, 2022). In past work, at high D/T ratios ($\geq$0.5), the just-suspended speed for solids suspension in a baffled square tank agitated by an HE-3 impeller was found to be lower than that in a cylindrical baffled tank (Mitchell et al., 2008). This was due to flow reversal, where a fillet forms beneath the impeller reducing suspension efficiency, which did not occur as readily in the square tank (Mitchell et al., 2008). Few publications are available focusing on the difference between square and cylindrical cross-section stirred tanks with respect to power, mixing and flow. Consideration of systems with different mixing mechanisms, like shaken well reactors have found that the corners of square cross-sections induced further turbulence and mass transfer (Duetz et al., 2000; Hermann, Lehmann and Büchs, 2003). Micheletti et al. (2006) determined that k_La values in deep square well plates were 30 % higher than that of standard round well plates. CHO cells cultured in square and cylindrical orbital shaken reactors were found to have similar growth kinetics when cultured at a lower agitation rate in the square reactor, implying similar mass transfer at lower speeds (Stettler et al., 2007).

In standard cylindrical tanks, studies on EE impellers are more common in down-pumping (DP) mode, particularly for microcarrier suspension applications (Collignon et al., 2010a; Collignon and Dossin, 2010b; Rotondi et al., 2021; Wyrobnik et al., 2022). Fewer studies characterise the EE impeller in both UP and DP mode (Simmons et al., 2007; Zhu et al., 2009; Collignon et al., 2016). CFD studies on the Ambr® 15, a non-standard STR geometry operating in the transitional regime, indicated that similar flow structures were achieved to that of the EE impeller in up-pumping (UP) mode in a traditional baffled cylindrical tank (Nienow et al., 2013). A study comparing axial impeller performance of the Mixel TTP, Lightnin A315 and A310, VMI-Rayneri and EE impellers for microcarrier suspensions found that the EE impeller (DP) achieved the just-suspended condition, N_{JS}, at significantly lower agitation rates than the alternative impeller designs investigated (Collignon et al., 2010a). Moreover, the average shear rate measured was lowest for the EE impeller, an important attribute when dealing with shear sensitive microcarrier adherent cells (Collignon et al., 2010a). For meeting mass transfer requirements at higher cell densities, UP mode is sometimes recommended for the EE impeller, where the large blades generate strong up-flow for air dispersion (Zhu et al., 2009; Nienow, Isailovic and Barrett, 2016).

The focus of this study is the development of a scale-down prototype of the Allegro™ STR 50–2000 L SUB range, with the aim of providing a bench-scale mimic of industry conditions for characterisation of power consumption, mixing, and flow dynamics. By developing a transparent 1 L scale-down prototype, resolution issues associated with the opacity and large volumes of commercially available large-scale STRs are avoided, allowing for mixing and flow dynamics characterisation across the global flow field. Moreover, a standard cylindrical STR of equivalent proportions operating with the same EE impeller is characterised for comparison of power consumption, flow structure, and mixing efficiency with that in the A-STR. This comparison aims to provide insight into how the unique geometry of the A-STR influences the flow and mixing dynamics of the EE impeller, which is the current impeller selection in the Allegro STR range. Due to its low shear properties, the EE impeller is used in many commercial bioreactors including the Ambr® 15 and new Ambr® 250 (Sartorius), the BIOSTAT® B-DCU range (Sartorius), as well as Eppendorf's New Brunswick™ Celligen® BLU and BioBlu range.

2. Materials and methods

2.1. Bioreactor configuration

A 1 L prototype (hereafter referred to as A-STR) of the single-use Allegro STR 50–2000 L bioreactor range was fabricated from transparent acrylic, scaling-down from vendor disclosed dimensions of the Allegro STR 50 bioreactor (Pall Corporation, Portsmouth, United Kingdom). Characteristic ratios (D/T = 0.5, C/T = 0.25, W/D = 0.5) of the vessel (Fig. 1) were maintained with scale-down, and acrylic inserts in each corner were used to mimic the bevelled effect created by the biocontainer support structure during operation. It should be noted that once fully inflated the Allegro STR single-use biocontainer is fully rigid and adherent to the supporting structure. These characteristics are therefore well captured by the rigid and scaled down transparent prototype manufactured for this work.

The maximum working volume V_L = 1 L (H_L/T = 1.1) is used as a reference condition for the characterisation study. Other liquid height to tank diameter ratios ranging from H_L/T = 0.6–1.1 are evaluated in UP mode to determine the influence on impeller power number. Wedge-shaped baffles are located on three of the four vessel faces. This asymmetric arrangement provides an open front-viewing screen during operation and practicality of biocontainer installation in industrial applications. Baffle width to tank diameter ratio, B_W/T = 0.1, with a maximum baffle thickness of 30 mm against the tank wall. The 3 bladed, 45° pitched Elephant Ear impeller was 3D printed with semi-transparency and high rigidity on a Form 3 printer (Formlabs, USA) using Stereo-Lithography (SLA) with a clear acrylic-based resin. The impeller was printed to a diameter of 50 mm, with a blade height W = 25 mm and a blade thickness of approximately 1.4 mm. Wet and dry sandpaper (1200 grit) was used for smoothing of impeller blades after the 3D-printing process. For comparison with a 'standard' STR geometry (hereafter referred to as S-STR), a dished bottom cylindrical tank with the same impeller design and characteristic ratios of the A-STR was used for characterisation studies. Four standard rectangular baffles of width B_w/T = 0.1 and 2 mm thickness were used in the cylindrical vessel. A hemispherical dished bottom was used, rather than a flat bottom configuration, given that the dished bottom is more common in commercial bioreactors (Schirmer et al., 2021). Some examples of cylindrical dished bottom bioreactors available commercially are the Sartorius Univessel (Wyrobnik et al., 2022), Mobius CellReady (Kaiser, Eibl and Eibl, 2011), and XCellerex XDR.

In both the A-STR and S-STR in this work, anti-clockwise impeller rotation is used for up-pumping (UP) agitation mode, and the contrary for down-pumping (DP) mode. The scale-down design has a top-mounted driven impeller, which deviates from the original bottom-mounted magnetically driven impeller design, for practicality and accessibility during characterisation studies. The main motivation for this was to fit into a frictionless air bearing base used in impeller power number characterisation and for ease

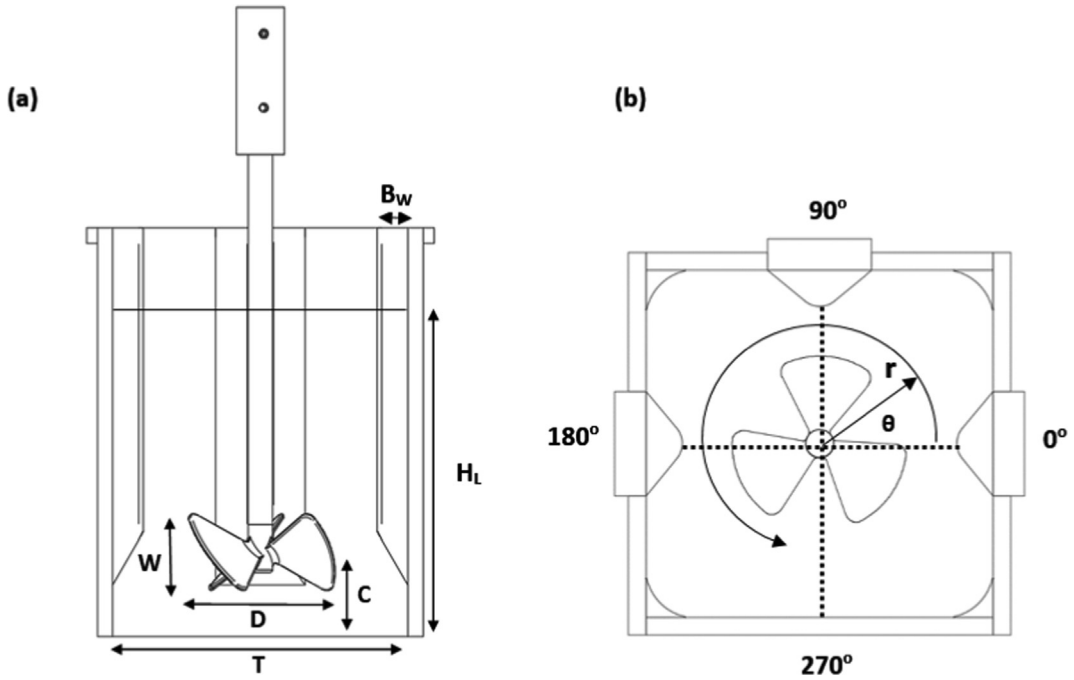

Fig. 1. Schematic diagram of the scale-down 1 L Allegro STR (A-STR) bioreactor prototype (a) side view (b) top view; dashed lines represent vertical PIV measurement planes (θ = 0°, 90°, 180°, 270°). Counterclockwise (CCW) rotation corresponds to UP mode and vice versa.

of access when carrying out particle image velocimetry (PIV) studies. The impeller was driven by a servo motor mounted onto plates supported from the vessel base, connected to an Ultra 3000 drive and controlled using Ultraware software (Rockwell Automation, USA).

2.2. Power consumption

The power curve of the 3-bladed Elephant Ear impeller in the ungassed A-STR vessel was acquired using a frictionless air-bearing system. The copper air-bearing was supplied with pressurised air at 0.25 bar to eliminate friction and allow free rotation of the tank. Impeller power input was determined using a digital force gauge (Model DFG55-0.12, Omega Engineering, UK). The power curve was obtained from the laminar ($Re \sim 1$) to turbulent ($Re \sim 2.4 \times 10^4$) regimes by varying the impeller agitation rate and working fluid rheological properties (Eq. (1)).

$$Re = \frac{ND^2\rho_L}{\mu} \tag{1}$$

Where N is the impeller agitation rate, ρ_L is the liquid density, and μ is the liquid dynamic viscosity. Milli-Q ultrapure water or mixtures of Milli-Q water and glycerol (99 % purity, Fisher Scientific, UK) were used as the working fluid. Higher glycerol concentrations allowed for measurements at low Re by increasing the viscosity. Density and viscosity of Milli-Q water/glycerol mixtures at each glycerol concentration were determined based on glycerol/water volume ratios and working temperature (Cheng, 2008). A wired digital thermometer (RS pro K-Type 1319A, RS Components, UK) was used to monitor the temperature at each condition for density and viscosity calculations. This was particularly important at higher glycerol concentrations where rapid agitation caused a notable temperature increase, influencing fluid properties and in turn Reynolds number (Re). Between adjustments of impeller agitation rate, a 3 min period was allowed for the flow in the bioreactor to reach steady state. The air bearing was then rotated away from the force gauge, which was subsequently tared, and the air bearing released. A 60 s initialisation period avoided measurements being taken while the vessel initially rebounded against the force gauge. After the initialisation period, measurements were averaged over 60 s at a frequency of 7000 Hz. The average force (n = 3 experimental repeats) measured at each condition was used to determine the power input, P (Eq. (2)) and consequently the impeller power number, N_P (Eq. (3)).

$$P = 2\pi NlF = 2\pi NT_q \tag{2}$$

$$N_P = \frac{P}{\rho_L N^3 D^5} \tag{3}$$

Where *l* is the lever arm and F the measured force – the product of which is the torque. The force gauge was clamped to a static motor support structure throughout measurements, and the perpendicular distance from the gauge arm to the central impeller shaft used as the lever arm. A spirit level was used to ensure the STR and force gauge were levelled throughout the force readings.

2.3. Flow dynamics

Particle image velocimetry (PIV) measurements were acquired using a pulsed Nd:Yag laser (Nano L 50–100, Litron, UK) with a power output rating of 2 × 50 mJ and wavelength λ = 532 nm. A cylindrical lens was used to convert the laser beam into a vertical laser sheet of approximately 1 mm thick. PIV experiments were carried out in four vertical planes of the tank (Fig. 1b) to measure the two-dimensional (2D) axial and radial velocity components in each plane. A cylindrical measurement system (r, θ, z) was employed, with the origin positioned at the centre of the tank bottom and the azimuthal coordinate, θ, increasing anticlockwise when viewed from above. Measured planes were located at θ = 0°, 90°, 180° and 270°. A high resolution 2048 × 2048 pixel camera (PowerView™ Plus 630091, TSI, USA) was positioned perpendicularly to the light sheet. The camera was fitted with a 60 mm lens (AF Micro-Nikkor, Nikon, Japan) and connected to a Laserpulse timing box (Model 610036, TSI Inc., USA), which was

controlled using Insight 4G™ Software (TSI Inc., USA) to sync camera and laser trigger times. The tank was seeded with rhodamine-coated polymethyl methacrylate particles of 1–20 μm diameter (Dantec Dynamics A/S, Denmark). Seeding particles were added in increments to obtain 10–15 particles per interrogation cell. The working fluid used was Ultrapure Milli-Q water, given the water-like viscosity and density of fed-batch mammalian cell culture at typical cell densities. To improve image clarity a 527–532 nm band-pass filter was fitted to the camera lens. The impeller and shaft were spray-painted with a black coating under a fume hood and left to dry prior to the experiment to minimise light reflection from the laser sheet. A timestep between image pairs of 0.7 ms was chosen for the agitation range of 220–250 RPM. This timestep was selected in line with standard PIV procedure to achieve a particle displacement of approximately ¼ of the interrogation cell grid length between image pairs in line with standard PIV procedure (Raffel et al., 2018).

PIVlab software (Thielicke and Sonntag, 2021) was utilised to pre-process the raw images by subtracting background images and applying contrast limited adaptive histogram equalisation (CLAHE) for improved visibility. A two-pass adaptive correlation analysis was carried out on PIVlab with an initial window size of 32 × 32 pixels, and a final window size of 16 × 16 pixels with 50 % interrogation area overlap (resulting in a final resolution of 8 × 8 pixels). The spatial resolution achieved was 4×10^{-4} m. Post-processing on PIVlab involved image filtering and velocity based validation. The instantaneous velocity fields derived from analysis of 3000 image pairs by PIVlab were used to obtain the mean (ensemble-averaged) velocity. Instantaneous velocity fields were extracted from PIVlab and processed using a purposely written MATLAB code. The kinetic energy, k, was estimated according to Eq. (4).

$$k = \frac{3}{4}\left(u_r'^2 + u_z'^2\right) \tag{4}$$

Where u_r and u_z refer to the radial and axial velocity components in the 2D plane considered, with the notations u_r' and u_z' referring to the ensemble-averaged standard deviations of the respective velocity components. The contribution of the third (tangential) velocity component was estimated as the average of the other two measured components:

$$u_\theta'^2 = \frac{u_r'^2 + u_z'^2}{2} \tag{5}$$

This assumption of isotropy is common in the literature when estimating the kinetic energy from 2D velocity measurements (Charalambidou et al., 2023; Collignon and Dossin, 2010b; Simmons et al., 2007; Wyrobnik, 2022; Zhu et al., 2009among others). Comparison between estimates of k obtained from 2D approximations (Eq. (5)) and 3D measurements was carried out by Chung, Barigou and Simmons, (2007) for a pitched blade turbine impeller, and they report a maximum discrepancy between the two values of 10 %. As ensemble-averaged measurements were not resolved based on impeller position, the standard deviation of the velocity components in Eqs. (4) and (5) include not only the turbulent but also pseudo-turbulent velocity fluctuations as a result of the blade passage.

2.4. Mixing time

Mixing time of the A-STR was characterised using the Dual Indicator System for Mixing Time (DISMT) (Melton et al., 2010). This technique is based on a fast acid-base reaction between sodium hydroxide (NaOH) and hydrochloric acid (HCL) in the presence of two indicators – methyl red (MR) and thymol blue (TB). Indicator stock solutions of 1.38 mg/mL TB and 1.52 mg/mL MR were formed by dissolving indicator powder in ethanol (70 % v/v, Thermofisher, UK) on a magnetic stirrer. The addition of 4.67 mL/L TB and 4.27 mL/L MR to de-ionized water formed a solution which is red at pH < 6, blue at pH > 8, and yellow for 6 < pH < 8 (Rodriguez et al., 2014). The dual-indicator solution was prepared to a volume of 1 L on a magnetic stirrer. Subsequently, NaOH was added in 5 μL increments until a pH of approximately 7.0 was measured using a pH probe (Mettler Toledo, USA), at which point the solution was bright yellow. The solution was added to the STR and the desired agitation rate set. A homogenous illuminated 580 mcd LED panel was placed behind the tank to improve image clarity and obtain a background of uniform intensity. Acidification of the solution by addition of 75 μL HCL (0.75 M), was followed by a two minute waiting time to ensure homogeneity. An iCube camera (NET, Germany) focused on the front tank face was set to start recording at a frequency of 25 Hz. To initiate the acid-base reaction and ensure consistency throughout experiments NaOH was added to the liquid surface from a chosen fixed port in the vessel lid (r = 46 mm; θ = 215°). Two minutes were allowed to pass to ensure the solution was fully mixed, and the capture of images stopped.

While stoichiometric amounts of base (neutralisation method) were added to the tank in initial experimental runs, a fast colour change from red to a homogenous grey/green state was observed, followed by a gradual colour change to yellow. When using the neutralisation method it has been reported that the resulting colour change yields the micro-mixing time, however, as in the current work, at acid-to-base ratios above two the colour change is representative of macromixing (Godleski and Smith, 1962; Cabaret et al., 2007). Micro-mixing times are important in process design where rapid chemical reactions are concerned, however, when considering homogeneity in the cell culture environment, macro-mixing characterisation is better suited. To obtain the macro-mixing time, an addition of 35 μL NaOH was thus used, for an acid-to-base ratio above two. After recording the colour change, the remaining stoichiometric NaOH quantity was added to neutralise the solution, followed by re-acidification with HCl to prepare for the next measurement. The dual indicator solution was changed with fresh solution after every three measurements, as colour changes after three sets of acidification and neutralisation were observed to be less reproducible.

Mixing was investigated across an agitation range of N = 100–500 RPM (Re ~ $4x10^3$-$2x10^4$) in the A-STR to cover a power input range of 3–350 W/m^3, in line with that of the commercial Allegro STR bioreactor range. At each agitation rate, n = 3 repeats were carried out to reduce statistical error associated with the turbulent dispersion process and the tracer injection protocol. For comparison of dimensionless mixing number (Nt_m), in the turbulent regime, mixing in the S-STR was investigated across a range of Re ~ $1x10^4$-$2x10^4$. The RGB images, which fully captured the colour change induced by the acid-base reaction, were processed using an in-house developed MATLAB code. This defines the mixing time based on the point at which 95 % homogeneity is achieved, rather than relying on estimates of mixing time based on visual observation as often associated with colorimetric techniques (Rodriguez et al., 2014). Two methods are used to determine the mixing time using the acquired images (Fig. 2).

Firstly, the standard deviation of the green pixel intensity across the plane of view was monitored and the mixing time determined from the point at which the standard deviation of the green pixel intensity dropped to below 5 %. Secondly, mixing time was determined based on the point at which 95 % of pixels in the viewing plane were mixed, where a pixel was considered mixed upon reaching 95 % of its final intensity. While the standard deviation method is a measure of instantaneous homogeneity across the field of view, the sigmoidal curve acquired from the percentage method takes into account local variation in mixing due to local velocity

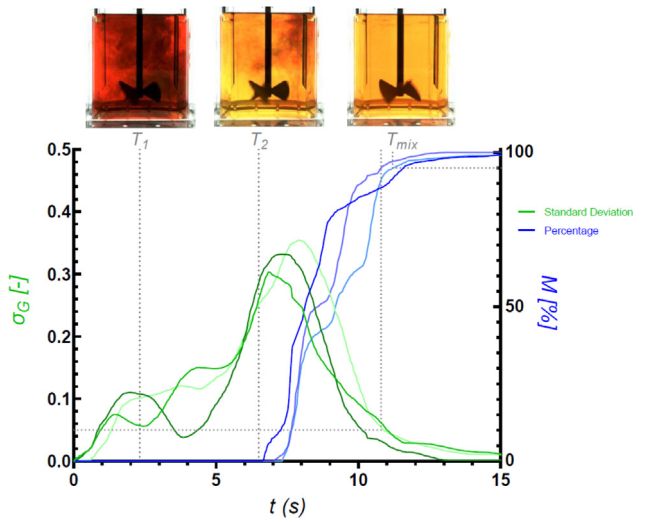

Fig. 2. Time evolution of the standard deviation of green pixel intensity, σ_G, and of the percentage of mixed pixels, M, after injection of base to an acidified DISMT solution in the A-STR (UP) at 100 RPM (3 W/m^3). Curves of different shades represent three experimental repeats. (For interpretation of the references to colour in this figure legend, the reader is referred to the web version of this article.)

variation and therefore mass transfer (Rodriguez et al., 2014). In the current work the final mixing time was estimated from the average of the two methods. To account for the inherent variation in colour intensity across the field of view associated with varied fluid depth relative to the camera position, the green intensity level of each pixel is normalised according to Rodriguez et al. (2014).

3. Results and discussion

3.1. Impeller power number

Impeller power input is one of the most significant parameters for bioreactor design and process scale-up, given its association with mixing and circulation times, heat and mass transfer, solids suspension, and viscous stresses, which can affect shear sensitive organisms (Ascanio, Castro and Galindo, 2004; Mollet et al., 2004; Kaiser et al., 2017). Most single-use bioreactors have bespoke impeller designs and are not easily comparable with traditional reusable configurations (Kaiser et al., 2017). Moreover, impeller power number can change significantly depending on factors like impeller diameter, impeller clearance, blade thickness, and baffle design (Chapple et al., 2002; Kaiser et al., 2017; Wyrobnik et al., 2022). The relationship between impeller power number and Reynolds number (Re) correlates strongly for different impellers in each flow regime, and the resulting plots are generally independent of scale for systems of similar geometry (Nienow, 2014). The novel geometries of single-use bioreactors makes the study of power input in these vessels particularly important, especially given that scale-up in mammalian cell culture systems is usually based on maintaining constant specific power input (P/V) (Langheinrich and Nienow, 1999; Junker, 2004; Xing et al., 2009). Characterisation of impeller power number in this work aims to provide a reliable means of scale-up maintaining power input, while also considering how power number will change across the characterised configurations. The power curves of the 3-bladed 45° pitched Elephant Ear (EE) impeller investigated in this work are presented in Fig. 3.

Impeller power number was investigated across a range of Re = 1.0–2.5x10^4 in the A-STR geometry to observe the change in power number from the laminar to turbulent regime. Throughout the

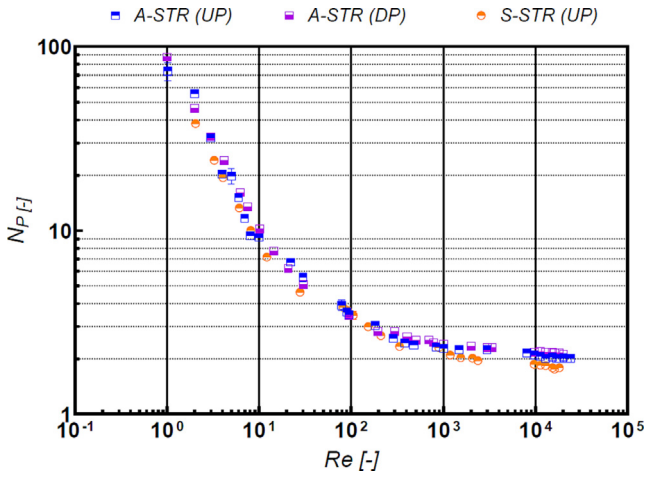

Fig. 3. Comparison between power curves of the EE impeller in UP (⬒) and DP (⬓) modes in the A-STR against that of a standard cylindrical configuration in UP mode (◓). Error bars represent standard deviation from the mean (n = 3).

laminar to turbulent regimes, the power curves of the EE impeller in the A-STR (UP and DP) and S-STR (UP) exhibit similar behaviour with increasing Re. For Re > 1×10^3, the A-STR (DP) exhibited the highest power numbers, followed by the A-STR (UP). Given that industry scale stirred tanks are almost exclusively operated in the turbulent regime for suspended cell culture applications, the turbulent power number is generally used to characterise such bioreactors. N_P of the 1 L A-STR is compared to that of the S-STR in both UP and DP mode in the turbulent regime (Fig. 4). N_P of the unbaffled A-STR (UP) is also presented to determine the influence of the square A-STR cross-section.

The turbulent power number of the A-STR was determined to be N_P = 2.11 ± 0.01 in UP mode and 2.17 ± 0.02 in DP mode. The corresponding values for the Allegro STR 200 L reactor were N_P = 1.93 ± 0.4 (UP) and 2.19 ± 0.2 (DP) (Pall Corporation, UK). The discrepancy between the two scale values in DP mode (2.11 vs 1.93) is well within the error range at 200 L scale (±0.4, ± 21 %). The agreement of power number indicates good scalability for operation in single-phase, however, industrial applications are

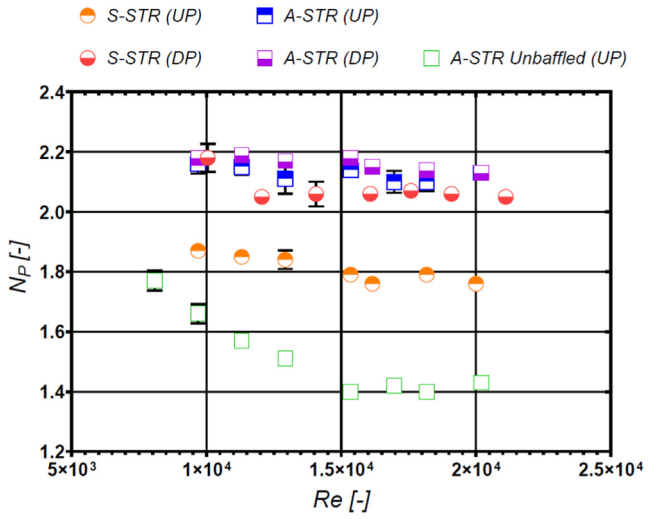

Fig. 4. Comparison of EE impeller turbulent power number in UP (⬒) and DP (⬓) modes in the A-STR with that of a standard cylindrical configuration (S-STR) in UP (◓) and DP (◒) modes. Unbaffled A-STR in UP mode (□) plotted to assess natural baffling of square cross-section. Error bars represent standard deviation from the mean (n = 3).

generally characterised by multiphase flow. Past characterisation of the EE impeller has shown that the turbulent power number is relatively independent of air flow rate in UP mode (Zhu et al., 2009). However, in DP mode impeller flooding occurred at higher air flow rates, causing a 30 % drop in power number (Zhu et al., 2009). Whether the same will occur in the Allegro STR geometry is uncertain, given that the distribution of gas outlets in its ring sparger may reduce flooding when compared to the sparger used by Zhu et al. (2009). Operation of the A-STR (UP) without baffles was characterised by a significantly reduced power number, by almost 34 % (Fig. 4). N_P in the unbaffled configuration plateaued at $N_{P\sim}$ 1.4 for Re > 1.5×10^4. This is indicative of the natural baffling provided by the square cross-section. Operation without baffles would typically result in a continually decreasing power number with increasing Re, rather than the constant turbulent power number typically seen in baffled tanks. For example, operation of an unbaffled SmartGlass bioreactor stirred by a combination of a top mounted EE impeller and a tapered disc blade turbine resulted in a continuously decreasing power number (Kaiser et al., 2017). The same power number decrease was observed in an unbaffled tank agitated by a Rushton turbine (Bujalski et al., 1987). This is to be attributed to the solid body rotation present in unbaffled stirred tanks (Kaiser et al., 2017), which is known to result in poor mixing (Ciofalo et al., 1996). The natural baffling provided by the cross-section of the Allegro STR bioreactor and the consequent plateau of the power number with increasing Re indicates the benefit of this novel geometry in reducing unwanted tangential flow and central vortex formation. In fact, N_P in the A-STR was 16.6 % higher than that in the S-STR (N_p = 1.81 ± 0.04), due to the combined influence of the baffles and the additional disturbance of flow provided by the tank corners in UP mode. In DP mode, the power number of the S-STR (2.09 ± 0.04) was more similar to that of the A-STR (2.17 ± 0.02). Analysis of the flow structures in both configurations (Section 3.2.1) will provide further insight into this aspect. Simmons et al. (2007) determined that NP = 1.7 for an EE UP impeller in a flat-bottomed, cylindrical STR (D/T = 0.45, C/T = 0.25, H_L/T = 1, W/T = 0.233). The slightly lower power number of the S-STR in this work is likely due to the difference in vessel geometry (flat vs round bottom) as well as the slightly larger impeller in the present work (D/T = 0.5, W/T = 0.25). N_p of the S-STR (DP) is in agreement with the value of 2.1 determined by Zhu et al. (2009) for a DP EE impeller. The Ambr® 250 equipped with a similar down-pumping 45° pitched Elephant Ear impeller (D/T = 0.5) was found to have a lower power number of N_p = 2.01 (Rotondi et al., 2021). The lower power number of the Ambr® 250 compared to the S-STR in this work is likely due to the absence of baffles in the Ambr® 250, although some baffling is provided by the large probes.

Keeping cell culture applications in mind, it is worth noting that the A-STR is operating in the turbulent flow regime at relevant power input for this bioreactor range. Animal cell culture is generally run with a specific power input of 10–150 W/m^3 (Nienow, 2006) and a power input of 50 W/m^3 was recommended for mAbs production in the Allegro STR 50 L bioreactor (Schirmer et al., 2020). Power number data obtained across the laminar to turbulent regimes for the A-STR (Fig. 3) indicated that at the theoretical threshold for turbulent flow, the A-STR was operating at an agitation rate of N = 240 rpm with a specific power input of *circa* 45 W/m^3. The threshold Reynolds number at which the flow regime becomes fully turbulent, where power number is independent of Re, is not strictly defined but generally assumed to be above Re = $1\text{x}10^4$–$2\text{x}10^4$ (Chapple et al., 2002; Nienow et al., 2013). This is key, given that regardless of vessel size, flow structures and spatial distribution of non-dimensional turbulent energy dissipation rate are conserved with scale when operating in the turbulent regime and vessel geometry is maintained (Nienow et al., 2013). This implies that the turbulent flow structures characterised in the 1 L scale A-STR at cell culture relevant power input are qualitatively comparable to those in the industry scale STR range.

Although impeller operation in both pumping directions is characterised in this work, UP mode is presented here as the reference condition, which is generally used for the commercial Allegro STR bioreactor range. Considering that end-users of bioreactors are likely to operate at varied fill heights (H_L/T), for instance with lower initial volumes in fed-batch cell culture, impeller power number in UP mode is characterised across a range of liquid heights in this work (Fig. 5).

The range of H_L/T = 0.6–1.1 corresponds to operation with 50–100 % of the 1 L maximum working volume. Fig. 5 shows that decreasing H_L/T from 1.1 to 0.8 caused a minor decrease in power number, as found in EE impeller studies by Simmons et al., 2007; Wyrobnik et al., 2022. However, at H_L/T = 0.7, there was an unexpected increase to N_P = 2.28. Further reduction of the fill height to H_L/T = 0.6 resulted in significant variation of power number across the investigated range of Re. At low Re (<11 000), N_P increased when compared to a fill volume of H_L/T = 0.7, however for Re > 11 000 a significant drop in power number occurred due to bubble entrainment. These aspects will be further discussed in Section 3.2.1 to follow.

3.2. Flow dynamics

3.2.1. Global flow field

A description of the single-phase flow occurring in the A-STR and S-STR is provided in this section. Ensemble-averaged velocity magnitudes were obtained in vertical planes from the centre of the tank to the four vessel faces (Fig. 1b) to capture the influence of the asymmetric baffle placement on flow dynamics in the A-STR. Planes are named from θ = 0-270° in the CCW direction (Fig. 1b) to differentiate between them. In the S-STR measurements were carried out in a single plane, given the tank symmetry with respect to the impeller shaft and assumed flow field symmetry. Axial and radial velocity components were used to determine ensemble-averaged velocity magnitudes at an agitation range of 220–250 rpm (Re ~ $1\text{x}10^4$-$1.1\text{x}10^4$), which corresponds to typical power input for suspended animal cell culture (~45 W/m^3). Impeller agitation rates in the A-STR and S-STR were adjusted across the aforementioned agitation range in order to have both vessels operating at the same volumetric power input. The normalised ensemble-averaged velocity magnitude and vector fields of the A-STR and S-STR configuration in up-pumping mode are presented in Fig. 6a, b and c, respectively.

Fig. 6c of the S-STR represents the typical velocity field exhibited by an EE impeller in UP mode. A primary recirculation loop

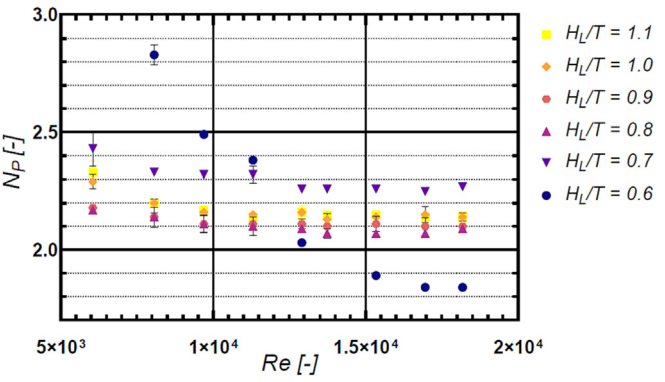

Fig. 5. Turbulent power number of the A-STR (UP) from 50 to 100 % fill volume, corresponding to liquid height to tank diameter ratios of H_L/T = 0.6–1.1.

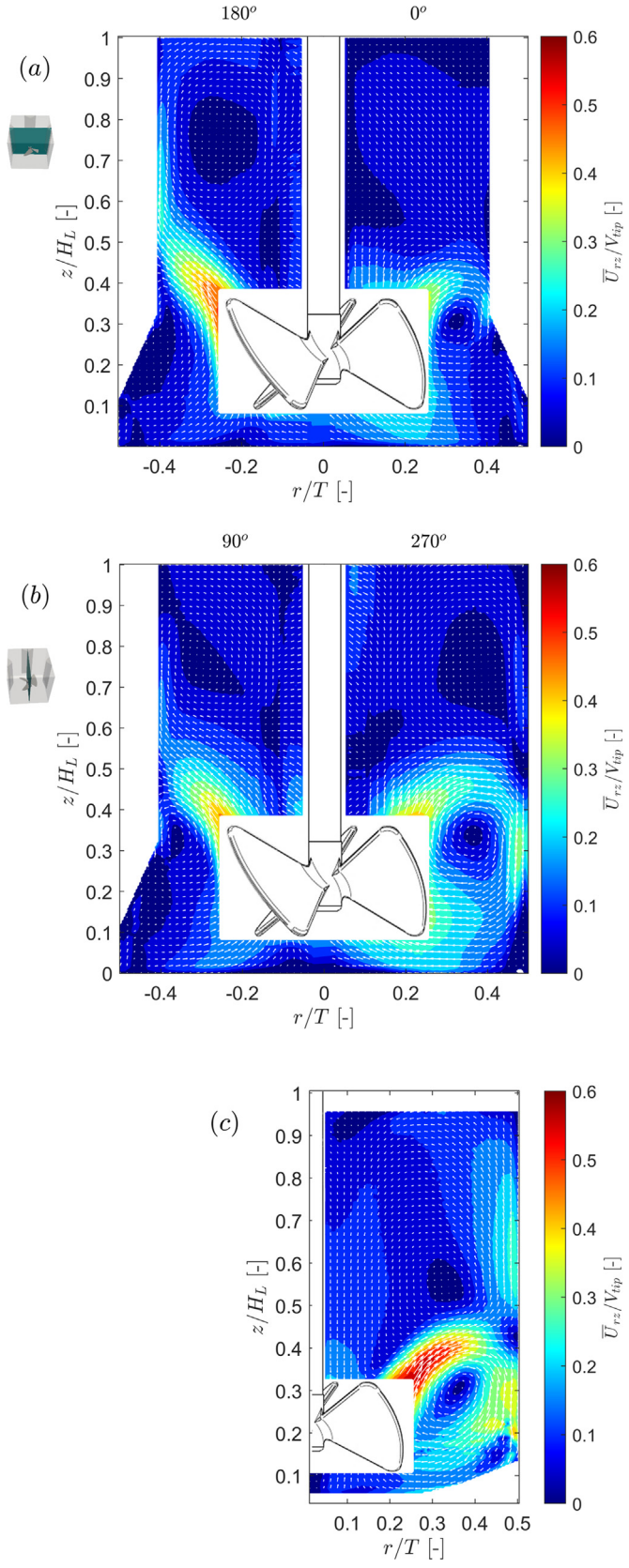

Fig. 6. Normalised ensemble-averaged velocity magnitude and vector map of the UP EE impeller (P/V ~ 45 W/m^3, Re ~ 1×10^4) in (a) A-STR (θ = 0°; 180°); (b) A-STR (θ = 90°; 270°); (c) S-STR.

of high velocity magnitude forms in the bottom half of the vessel, and a weaker anticlockwise circulation loop centred around z/H_L = 0.5 reaches the tank surface before rejoining with the primary loop in the impeller swept region. The primary recirculation loop reaches a height z/H_L = 0.48 (Fig. 6c). Velocities in the impeller discharge region have a maximum magnitude of 0.58V_{tip}. LES simulations of an UP EE impeller in a dished bottom cylindrical tank (D/T = 0.4; H_L/T = 1.24; C/H_L = 0.24) produced a similar ensemble-averaged velocity field with maximum velocities of approximately 0.6V_{tip} in the primary circulation loop (Collignon et al., 2016).

The velocity field in the A-STR is notably different from that in a standard STR due to the asymmetric baffle placement. In the plane at θ = 270° (perpendicular to the front unbaffled tank face) the flow structure is similar to that typically exhibited by an UP EE impeller. A strong recirculation loop is present in the lower half of the tank reaching z/H_L~ 0.5 with velocity magnitudes reaching 0.42V_{tip}. An anticlockwise recirculation loop is also present in the upper half of the tank with velocities below 0.15V_{tip}. Moving CCW in the direction of impeller rotation into the plane at θ = 0°, the upper anticlockwise circulation loop is no longer present. In the subsequent planes at θ = 90° and θ = 180° there is a more noticeable change in flow structure. The impeller discharge curves prominently upward in both of these planes, forming a large recirculation loop. In short, as the impeller rotates from the unbaffled tank face through subsequent baffled cross-sections, the direction of the impeller discharge stream at the tank wall (r/T > 0.4) changes orientation from the typical downwards to upwards. Similarly, the intensity of the impeller discharge stream varies significantly when considering the four different cross sections of the vessel. For example, the highest intensity is found at θ = 180° (0.48V_{tip} in the impeller discharge) while a lower maximum of only 0.27V_{tip} is present at θ = 0°. This change in intensity and direction must be related to the presence of baffles, which redirect the flow radially and axially and are consistent with previous work of Fan et al. (2021), who reported up to a 50 % increase in vertical plane velocity for a baffled configuration with a pitched blade turbine.

The ensemble-averaged velocity fields in the A-STR can help to further understand the unexpected increase in power number discussed (Fig. 5) when the free surface was reduced to z/H_L < 0.7. In fact, from Fig. 6a it is evident that the impeller discharge impinges on the wall at a height of z/H_L ~ 0.55 and the resulting upward stream reaches axial coordinates as high as z/H_L = 0.8. This implies that the increase in power number might be related to an interaction between the impeller discharge and the lowered free surface. It should be noted that this behaviour is characteristic only of the A-STR presented in this work, and for example a similar investigation by Simmons et al. (2007) did not report a power number increase when lowering the free surface in a cylindrical vessel. This again might be explained from Fig. 6c where it is evident that the impeller discharge is mainly reverted toward the bottom of the tank in the S-STR, and therefore would interact to a lower extent with the free surface even at reduced z/H_L.

Ensemble-averaged normalised velocity magnitude and vector maps of the A-STR (Fig. 7a, b) and the S-STR (Fig. 6c) are presented in down-pumping mode for comparison. Asymmetry in the flow field is less significant in the A-STR in DP mode when compared to that in UP mode. DP mode in the A-STR results in one large anticlockwise circulation loop generated by the EE impeller. Velocities in the lower half of the tank reach up to 0.52V_{tip} while the upper tank region (z/H_L > 0.5) exhibits lower velocities of up to 0.26V_{tip}. Velocities near the liquid surface of the A-STR are generally higher in DP mode when compared to UP mode. Comparison of UP (Fig. 6c) and DP (Fig. 7c) velocity fields generated in the S-STR

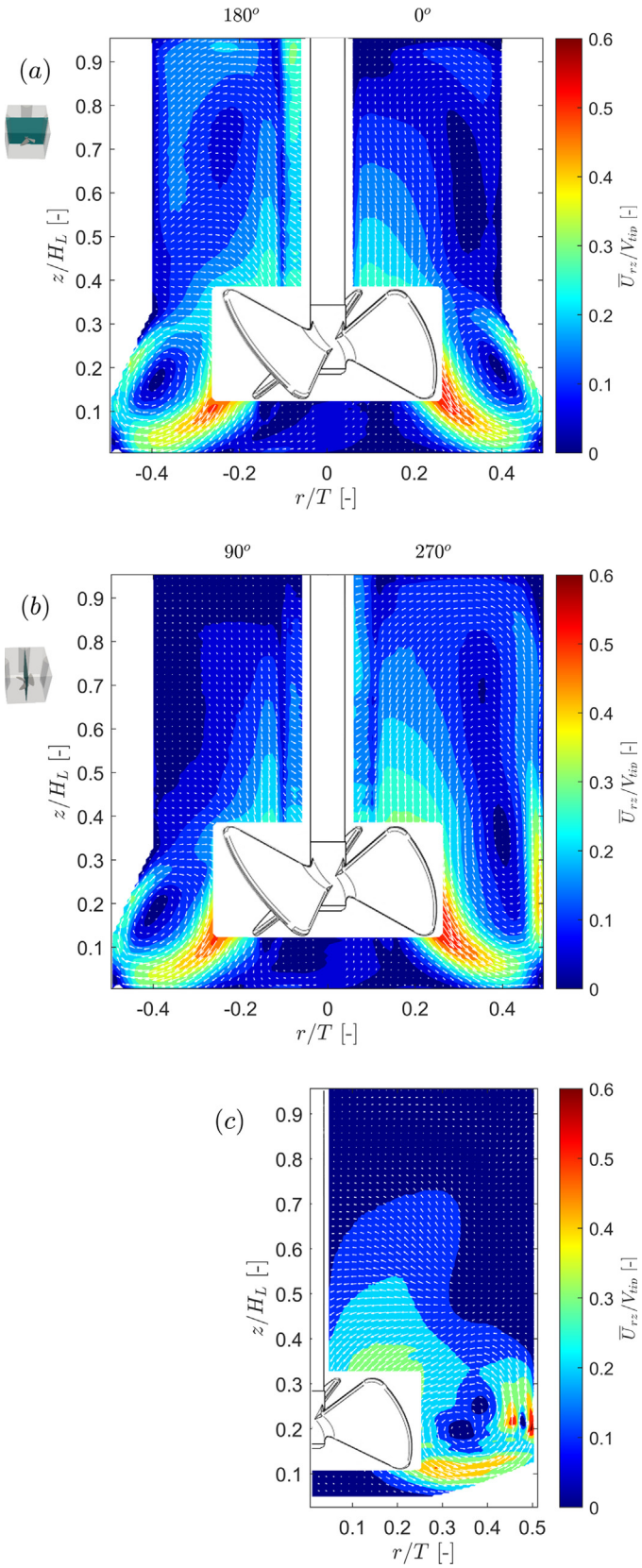

Fig. 7. Normalised ensemble-averaged velocity magnitude and vector maps of the DP EE impeller (P/V ~ 45 W/m^3, Re ~ 1x10^4) in (a) A-STR (θ = 0°; 180°); (b) A-STR (θ = 90°; 270°); (c) S-STR.

shows the opposite behaviour – velocities in the upper tank region are considerably lower in DP mode. Previous work had similar findings of poor circulation in the upper tank region in DP mode (Zhu et al., 2009). The EE impeller in the S-STR (DP) effectively has a lower impeller clearance due to the effect of the dished bottom, which may hinder impeller performance. The larger velocity magnitudes in the upper region of the A-STR (DP) compared to the S-STR (DP) may be due to the unbaffled tank face in the A-STR. Fig. 7a, b indicate that the planes at θ = 180° and θ = 270° contain circulation loops of higher velocities in the upper tank region ($z/H_L > 0.5$) when compared to the other two planes. As the impeller rotates CW in DP mode and passes through the plane at θ = 270° (perpendicular to the unbaffled front face) the lack of a baffle obstructing the flow results in a high velocity upward flow at the wall. High velocities in the upper half of the tank persist at the subsequent plane (θ = 180°) that the impeller rotates into. As the impeller passes through the baffled planes at θ = 90° and subsequently θ = 0°, there is a clear decrease in velocity magnitude in the upper tank region. The A-STR geometry appears to perform better in DP mode due to the unbaffled front face, given the improved circulation in the upper tank region when compared to the S-STR.

Flow field characterisation in this work is carried out in single-phase, however operation in multi-phase in industrial applications may result in changes in flow structure. Zhu et al. (2009) found that the lower circulation loop generated by an UP EE impeller was retained at high air flow rates, but with a more even spread of energy, while down-flowing liquid in the upper circulation loop was diverted to the tank wall rather than straight down to the impeller. In DP mode, formation of gas cavities behind the impeller blades caused shortening of the circulation loop, reducing liquid velocities and causing poorer circulation in the upper half of the vessel (Zhu et al., 2009). It was previously noted that the A-STR has a significantly higher power number than the S-STR in UP mode due to the combined effect of the baffles and disturbance of flow by the tank corners. However, N_P of the A-STR and S-STR in DP mode were relatively similar. This may be due to the raised height of the baffles in the A-STR, hence the impeller discharge in DP mode (Fig. 7a, b) does not interact with the baffles to as great an extent as in UP mode (Fig. 6a, b).

3.2.2. Kinetic energy distribution

Data acquired using the PIV system described in Section 2.3 was used to calculate (Eq. (4)) the ensemble-averaged kinetic energy (k) due to the combined action of turbulent and pseudo-turbulent (i.e. induced by the impeller blade and large-scale macro-instability) velocity fluctuations (Ducci and Yianneskis, 2007; Bouremel et al., 2009a, 2009b). k normalised with respect to V_{tip}^2 is presented in Fig. 8a, b for the A-STR (UP), while that in the S-STR (UP) is presented in Fig. 8c.

Contrary to the behaviour exhibited by the ensemble-averaged velocity field (Fig. 6a, b), the kinetic energy reaches its highest values at θ = 0° and θ = 270° (k = 0.095 V_{tip}^2). This might be explained by the fact that the kinetic energy shown in Fig. 8 also includes the pseudo-turbulent fluctuations related to the impeller trailing vortices. It is therefore expected that its intensity is highest along the unbaffled wall, where the organised flow of the trailing vortices is the least disturbed. As the impeller rotates CCW, the kinetic energy decreases as the baffles interact with the trailing vortices and redistribute their kinetic energy into the mean flow. The ensemble-averaged kinetic energy in the S-STR UP (Fig. 8c) reaches a maximum of 0.094 V_{tip}^2, similar to that in the A-STR. However, the

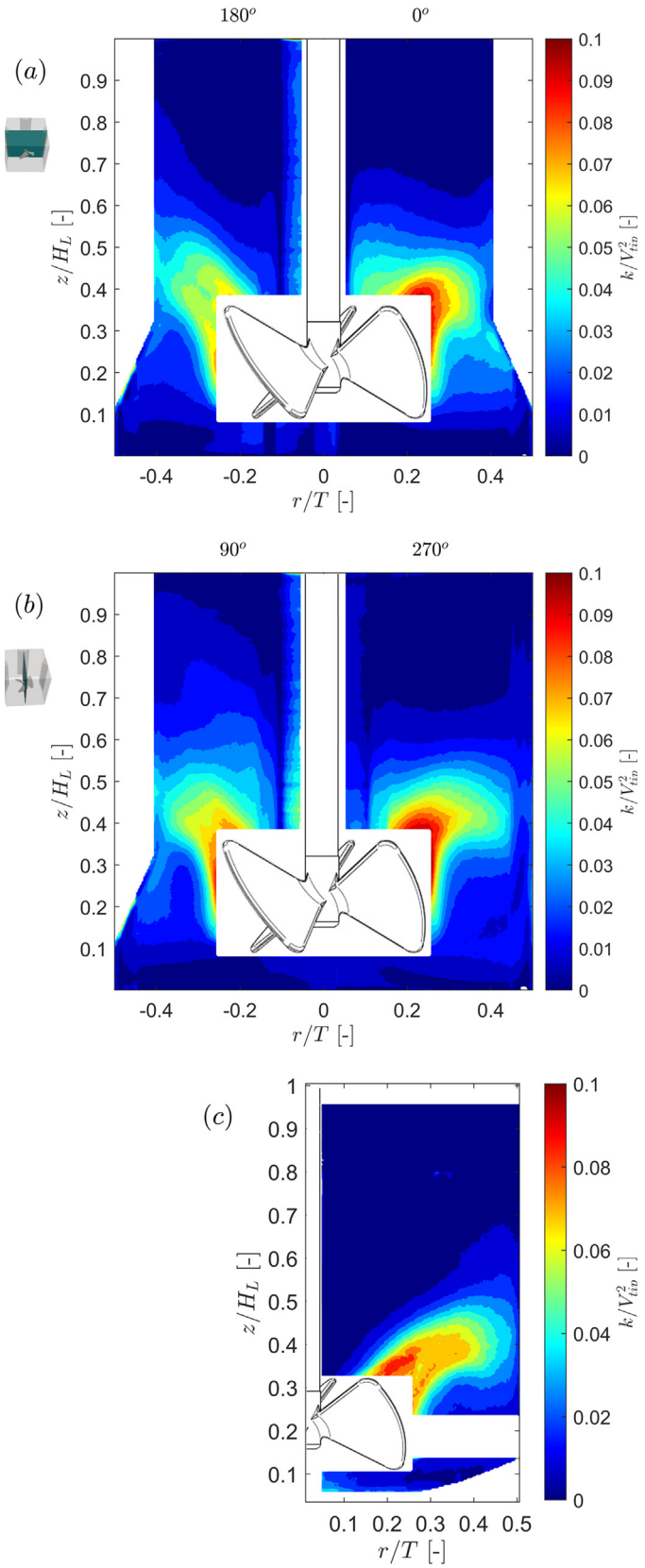

Fig. 8. Normalised ensemble-averaged kinetic energy due to turbulent and pseudo-turbulent fluctuations in an UP EE impeller (P/V ~ 45 W/m^3, Re ~ 1x10^4) in (a) A-STR (θ = 0°; 180°); (b) A-STR (θ = 90°; 270°); (c) S-STR.

S-STR has higher kinetic energy values extending to the tank peripheries. In the A-STR, planes at θ = 90° and 180° exhibit considerably lower maximum kinetic energy than the S-STR, with greater distribution of k in the upper half of the tank. In the S-STR kinetic energy is more localised to the impeller discharge region where z/H_L < 0.5 and r/T > 0.2. More homogeneous distribution of kinetic energy in the A-STR (UP) suggests better circulation and mixing.

Kinetic energy distribution is presented for the A-STR (DP) configuration in Fig. 9. When comparing the UP and DP configurations it is evident that k is significantly lower in the latter, with maximum values of $k = 0.067V_{tip}^2$ at θ = 0°. Moreover, kinetic energy in DP mode was more homogenously distributed throughout the tank planes, with higher magnitudes of up to $0.032V_{tip}^2$ near the liquid surface. The associated improved circulation in the upper half of the tank can be beneficial in avoiding cell exposure to spatial gradients, for instance, when pH buffers or feed are added via probes at the liquid surface.

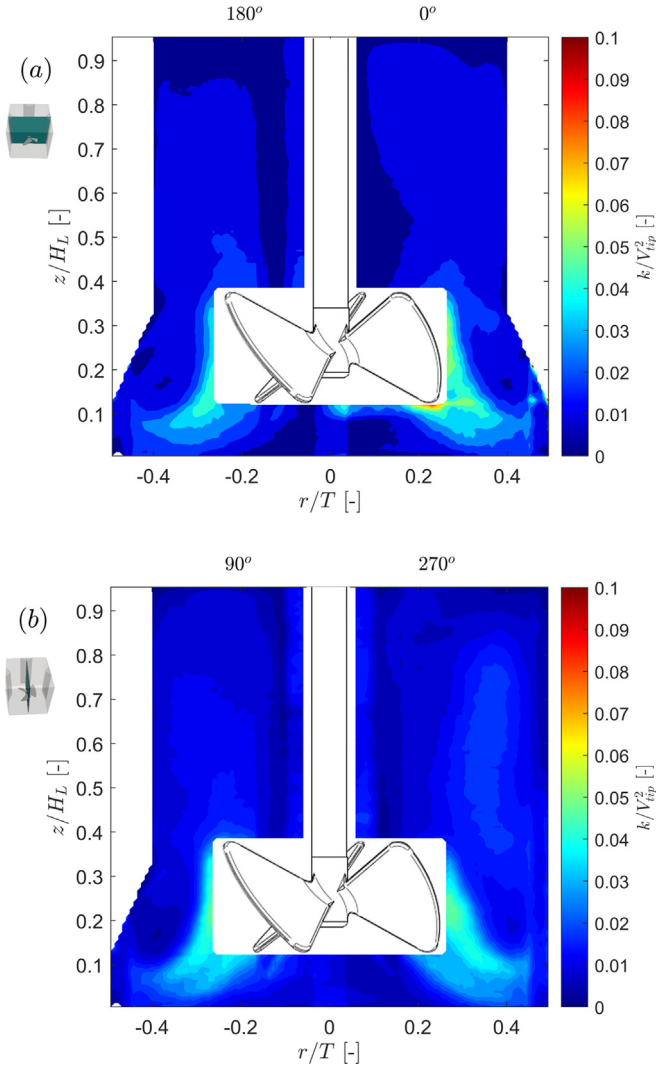

Fig. 9. Normalised ensemble-averaged turbulent kinetic energy of a down-pumping EE impeller (P/V ~ 45 W/m^3, Re ~ 1x10^4) in (a) A-STR (θ = 0°; 180°); (b) A-STR (θ = 90°; 270°).

3.3. Mixing dynamics

The final section of this work characterises mixing dynamics of the EE impeller in the A-STR and S-STR in the up and down-pumping modes. Mixing in the A-STR was investigated for impeller agitation rates in the range of 100–500 RPM (P/V = 3–350 W/m^3). As mixing time in STRs can vary considerably across the scale, comparison of mixing efficiency between vessels is better achieved using the non-dimensional mixing time, Nt_m. The non-dimensional mixing time represents the number of impeller revolutions to achieve a predefined fully mixed condition (usually 95 % homogeneity). Theoretically, it should remain constant with scale when maintaining geometric similarity and operating in the turbulent regime (Nienow, 1997). Mixing numbers of the A-STR and S-STR are compared in Fig. 10.

Mixing time data from a manufacturer characterisation study (Nienow, Isailovic and Barrett, 2016) were used to determine the non-dimensional mixing time of the commercial Allegro STR 200 L bioreactor in UP mode. Comparison with that of the 1L A-STR (UP) of the current work shows agreement of mixing numbers, indicating that geometric similarity was maintained with scale-down. The 1 L A-STR required 16.7 ± 1.7 impeller revolutions to reach 95 % homogeneity, while the STR 200 required 18.2 ± 2.5 revolutions. In the down-pumping A-STR the mixing number was lower at 11.3 ± 1.1 revolutions, however industry scale data in down-pumping mode was not available for comparison. Nienow (1997) mentions that mixing time correlations should hold under aerated conditions, given that the gassed impeller power number is used and impeller flooding does not occur. Given that Zhu et al. (2009) found EE impeller power number to be independent of air flow rate in UP mode, it is expected that the agreement of 1 L Nt_m data with industry scale data is expected to hold with multiphase operation. On average, mixing times in the A-STR in DP mode were approximately 32 % lower than in UP mode, implying more efficient single-phase mixing. The rapid mixing in the A-STR in DP mode correlates with the relatively high velocities in the upper half of the tank and well distributed kinetic energy when compared to the other configurations (cf. Figs. 7 & 9). In contrast, the S-STR (DP) had the longest mixing times, with Nt_m = 24.2. Poor circulation above z/H_L = 0.5 (Fig. 7c) is likely the cause of the inferior mixing performance in the S-STR (DP). Data regarding mixing times extracted from a study on EE impellers in down-pumping mode (Collignon et al., 2010b) in cylindrical tanks of 20, 80, and 600 L (H_L/T = 1; D/T = 0.5; C/H = 1/3; D_b = D/10) were used to calculated non-dimensional mixing numbers of approximately 9.6, 12.4, and 8.4, respectively. The lower mixing number compared to the current work is likely due to their higher impeller clearance. Wyrobnik et al. (2022) found that the mixing number of Bach, 3BS and marine impellers all decreased significantly when increasing impeller clearance from C/T = 0.33 to C/T = 0.55. Nt_m of the S-STR (UP) in this work is 16.9, in line with that of the A-STR (UP). Analysis of colour change images acquired using the DISMT technique can provide useful insight into global mixing in the vessel rather than reliance on probe measurements at a single location, which are also often limited by probe response times (Rodriguez et al., 2014). Mixing time distribution in the A-STR and S-STR in UP mode at moderate power input are compared in Fig. 11.

Distribution of mixing time is highly homogenous in the A-STR (Fig. 11a) with a slightly slower mixing region in the top right of the tank (z/H_L > 0.5; r/T > 0). This is unlike those seen in previous studies of this nature where symmetric mixing maps generally either show a slow mixing region around the impeller shaft or at the tank walls (Samaras et al., 2020; Wyrobnik et al., 2022). Flow dynamics characterisation in this work (Section 3.2) indicated min-

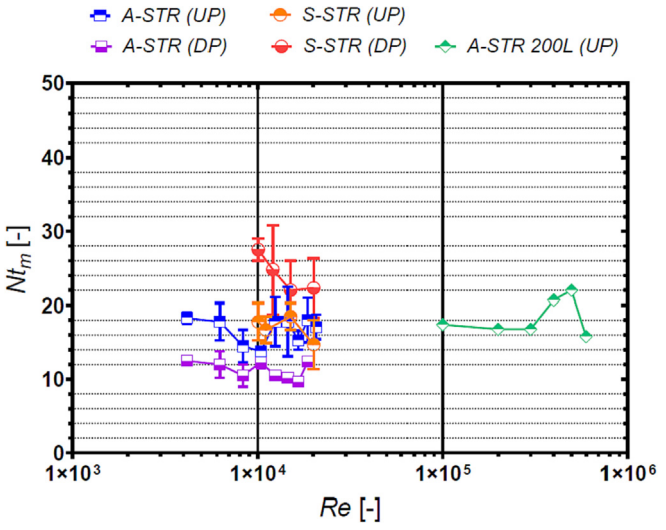

Fig. 10. Dimensionless mixing number, Nt_m, of the 1 L A-STR in UP (⬒) and DP (⬓) modes compared to that of the S-STR in UP (◓) and DP (◒) modes. Mixing time data on the commercial Allegro STR 200 L bioreactor (UP ◈) (Nienow, Isailovic and Barrett, 2016) is shown as an indication of the scalability of Nt_m.

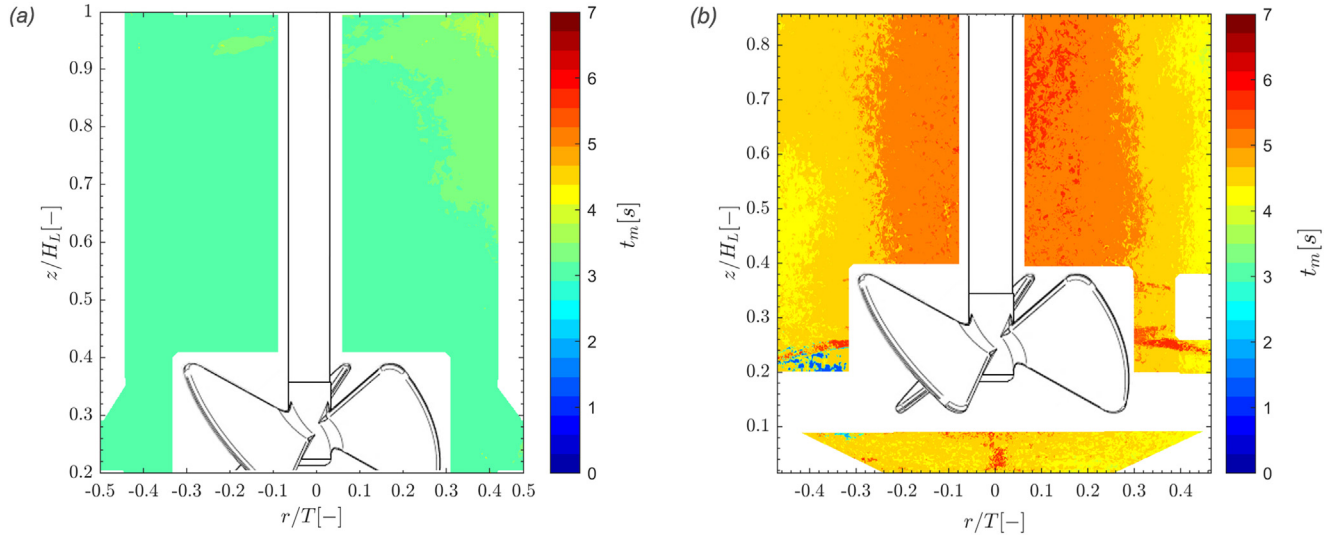

Fig. 11. Mixing time distribution in (a) A-STR, (b) S-STR at moderate power input (45 W/m^3).

imum velocities and kinetic energy at θ = 0° in the corresponding slower mixing time region. The addition of NaOH to initiate the colour change to a port on the opposite side of the vessel (r = 46 mm; θ = 215°) may have further contributed to the slightly slower mixing region in Fig. 11a. The mixing map of the UP S-STR (Fig. 11b) shows a less homogenous mixing map, with a prominent slow mixing region in the tank centre. While averaged dimensionless mixing numbers of the A-STR and S-STR are similar in UP mode, the mixing time distribution maps indicate more homogenous mixing in the A-STR when operated at typical power input (45 W/m^3). This is in line with the kinetic energy plot (Fig. 8c) which shows less homogenous distribution of kinetic energy in the S-STR. Unlike in the A-STR, kinetic energy in the S-STR is mostly concentrated in the impeller discharge region. Overall, the square cross-section and large baffles of the A-STR appear to improve distribution of kinetic energy, resulting in more homogenous mixing compared to the S-STR, particularly in DP mode.

4. Conclusions

Comparison of power and mixing number data with that of the industrial Allegro STR bioreactor range indicates that the scale-down A-STR can be seen as a suitable mimic of industry scale conditions. The A-STR was found to have higher power numbers in both up and down-pumping mode when compared to the S-STR configuration, with the square-cross section of the A-STR acting as an additional form of baffling. Ensemble-averaged velocity magnitudes in UP mode indicated an asymmetric flow structure due to the baffle placement in the A-STR, with higher velocities in the upper tank region $z/H_L > 0.5$ when compared to the S-STR. The ensemble-averaged kinetic energy had similar maximum values in the A-STR (UP) and S-STR (UP), with the A-STR exhibiting maximum k values in proximity to the unbaffled tank face. However, in the baffled region of the A-STR, kinetic energy is considerably lower than that in the S-STR. Overall there is a better distribution of kinetic energy in the A-STR (UP) compared to the S-STR (UP) which had high kinetic energy values in the impeller region and low kinetic energy values where $z/H_L > 0.5$ and $r/T < 0.3$. This was confirmed in mixing time distribution plots. Although the S-STR (UP) and A-STR (UP) did not differ significantly in average Nt_m values, the S-STR exhibited a less homogenous mixing time distribution, implying that cells are more likely to be exposed to spatial heterogeneities. The A-STR (DP) performed best in terms of mixing efficiency, exhibited well-distributed mean kinetic energy, and had strong recirculation loops reaching the tank surface. The Allegro STR bioreactor in DP mode should be particularly well suited to culture anchorage dependent cell types requiring microcarrier suspension, given its superior mixing performance and relatively low maximum kinetic energy. The superior performance of the EE (DP) impeller in the A-STR in this work when compared to the standard bioreactor configuration indicates that the combination of the EE impeller and A-STR geometry is likely to be highly favourable for culture of cells sensitive to shear and spatial gradients in pH, nutrients, and oxygen supply. The investigation in single-phase flow has revealed interesting features of the EE impeller, as well as new information on the influence of the Allegro STR geometry, however further work on multiphase flow operation would be beneficial to further explore the implications for industrial applications.

CRediT authorship contribution statement

J.N. Delbridge: Conceptualization, Methodology, Formal analysis, Investigation, Data curation, Writing – original draft, Writing – review & editing, Visualization. **T.A. Barrett:** Conceptualization, Writing – review & editing, Supervision, Project administration. **A. Ducci:** Conceptualization, Methodology, Formal analysis, Resources, Writing – review & editing, Visualization, Supervision. **M. Micheletti:** Conceptualization, Methodology, Writing – review & editing, Visualization, Supervision, Project administration, Funding acquisition.

Data availability

Data will be made available on request.

Declaration of Competing Interest

The authors declare that they have no known competing financial interests or personal relationships that could have appeared to influence the work reported in this paper.

Acknowledgements

The authors would like to acknowledge the funding and support of the University College London – Pall Corporation Centre of Excellence and the UKRI Engineering and Physical Sciences Research Council (EPSRC) CDT Bioprocess Engineering Leadership Grant EP/S021868/1. Further, the author gives thanks to the UCL mixing group – special thanks to Dr Anne De Lamotte for their training on power consumption, mixing and PIV experimental work as well as the provision of their MATLAB code written for DISMT analysis.

References

Ascanio, G., Castro, B., Galindo, E., 2004. Measurement of power consumption in stirred vessels-a review. Chem. Eng. Res. Des. 82 (9 SPEC. ISS.), 1282–1290. https://doi.org/10.1205/cerd.82.9.1282.44164.

Bouremel, Y., Yianneskis, M., Ducci, A., 2009a. On the utilisation of vorticity and strain dynamics for improved analysis of stirred processes. Chem. Eng. Res. Des. 87 (4), 377–385. https://doi.org/10.1016/j.cherd.2008.11.016.

Bouremel, Y., Yianneskis, M., Ducci, A., 2009b. Three-Dimensional deformation dynamics of trailing vortex structures in a stirred vessel. Ind. Eng. Chem. Res. 48 (17), 8148–8158. https://doi.org/10.1021/ie801481v.

Bujalski, W., Nienow, A.W., Chatwin, S., Cooke, M., 1987. The dependency on scale of power numbers of Rushton disc turbines. Chem. Eng. Sci. 42 (2), 317–326. https://doi.org/10.1016/0009-2509(87)85061-3.

Cabaret, F., Bonnot, S., Fradette, L., Tanguy, P.A., 2007. Mixing time analysis using colorimetric methods and image processing. Ind. Eng. Chem. Res. 46 (14), 5032–5042. https://doi.org/10.1021/ie0613265.

Chapple, D., Kresta, S.M., Wall, A., Afacan, A., 2002. The effect of impeller and tank geometry on power number for a pitched blade turbine. Chem. Eng. Res. Des. 80 (4), 364–372. https://doi.org/10.1205/026387602317446407.

Charalambidou, A.D., Micheletti, M., Ducci, A., 2023. Study of trailing vortices and impeller jet instabilities of a flat blade impeller in small-scale reactors. AIChE Journal 69 (2), 1–18. https://doi.org/10.1002/aic.17842.

Chen, P., Demirji, J., Ivleva, V.B., Horwitz, J., Schwartz, R., Arnold, F., 2019. The transient expression of CHIKV VLP in large stirred tank bioreactors. Cytotechnology Springer, Netherlands 71 (6), 1079–1093. https://doi.org/10.1007/s10616-019-00346-x.

Cheng, N.S., 2008. Formula for the viscosity of a glycerol-water mixture. Industrial Eng. Chem. Res. Am. Chem. Soc. 47 (9), 3285–3288. https://doi.org/10.1021/ie071349z.

Chotigeat, W., Watanapokasin, Y., Mahler, S., Gray, P.P., 1994. Role of environmental conditions on the expression levels, glycoform pattern and levels of sialyltransferase for hFSH produced by recombinant CHO cells. Cytotechnology 15 (1-3), 217–221. https://doi.org/10.1007/BF00762396.

Ciofalo, M., Brucato, A., Grisafi, F., Torraca, N., 1996. Turbulent flow in closed and free-surface unbaffled tanks stirred by radial impellers. Chem. Eng. Sci. 51 (14), 3557–3573. https://doi.org/10.1016/0009-2509(96)00004-8.

Collignon, M.-L., Delafosse, A., Crine, M., Toye, D., 2010a. Axial impeller selection for anchorage dependent animal cell culture in stirred bioreactors: Methodology based on the impeller comparison at just-suspended speed of rotation. Chem. Eng. Sci. 65 (22), 5929–5941. https://doi.org/10.1016/j.ces.2010.08.027.

Collignon, M.-L., Delafosse, A., Calvo, S., Martin, C., Marc, A., Toye, D., Olmos, E., 2016. Large-Eddy Simulations of microcarrier exposure to potentially damaging eddies inside mini-bioreactors. Biochem. Eng. J. Elsevier B.V. 108, 30–43. https://doi.org/10.1016/j.bej.2015.10.020.

Collignon, M.L., Dossin, D., et al., 2010b. Quality of mixing in a stirred bioreactor used for animal cells culture: Heterogeneities in a lab scale bioreactor and evolution of mixing time with scale up. Biotechnol. Agronomy Soc. Environ. 14 (SPEC. ISSUE 2), 585–591.

Ducci, A., Yianneskis, M., 2007. Vortex identification methodology for feed insertion guidance in fluid mixing processes. Chem. Eng. Res. Des. 85 (5 A), 543–550. https://doi.org/10.1205/cherd06192.

Duetz, W.A., Rüedi, L., Hermann, R., O'Connor, K., Büchs, J., Witholt, B., 2000. Methods for intense aeration, growth, storage, and replication of bacterial strains in microtiter plates. Appl. Environ. Microbiol. 66 (6), 2641–2646. https://doi.org/10.1128/AEM.66.6.2641-2646.2000.

Fan, Y., Sun, J., Jin, J., Zhang, H., Chen, W., 2021. 'The effect of baffle on flow structures and dynamics stirred by pitch blade turbine'. Chem. Eng. Res. Des. Inst. Chem. Eng. 168, 227–238. https://doi.org/10.1016/j.cherd.2021.01.017.

Godleski, E.S., Smith, J.C., 1962. Power requirements and blend times in the agitation of pseudoplastic fluids. AIChE J 8 (5), 617–620. https://doi.org/10.1002/aic.690080511.

Godoy-Silva, R., Chalmers, J.J., Casnocha, S.A., Bass, L.A., Ma, N., 2009a. Physiological responses of CHO cells to repetitive hydrodynamic stress. Biotechnol. Bioeng. 103 (6), 1103–1117. https://doi.org/10.1002/bit.22339.

Godoy-Silva, R., Mollet, M., Chalmers, J.J., 2009b. Evaluation of the effect of chronic hydrodynamical stresses on cultures of suspensed CHO-6E6 cells. Biotechnol. Bioeng. 102 (4), 1119–1130. https://doi.org/10.1002/bit.22146.

Hermann, R., Lehmann, M., Büchs, J., 2003. Characterization of gas-liquid mass transfer phenomena in microtiter plates. Biotechnol. Bioeng. 81 (2), 178–186. https://doi.org/10.1002/bit.10456.

Hsu, W.-T., Aulakh, R.P.S., Traul, D.L., Yuk, I.H., 2012. Advanced microscale bioreactor system: A representative scale-down model for bench-top bioreactors. Cytotechnology 64 (6), 667–678. https://doi.org/10.1007/s10616-012-9446-1.

Joe, C.C.D., Jiang, J., Linke, T., Li, Y., Fedosyuk, S., Gupta, G., Berg, A., Segireddy, R.R., Mainwaring, D., Joshi, A., Cashen, P., Rees, B., Chopra, N., Nestola, P., Humphreys, J., Davies, S., Smith, N., Bruce, S., Verbart, D., Bormans, D., Knevelman, C., Woodyer, M., Davies, L., Cooper, L., Kapanidou, M., Bleckwenn, N., Pappas, D., Lambe, T., Smith, D.C., Green, C.M., Venkat, R., Ritchie, A.J., Gilbert, S.C., Turner, R., Douglas, A.D., 2022. Manufacturing a chimpanzee adenovirus-vectored SARS-CoV-2 vaccine to meet global needs. Biotechnol Bioeng 119 (1), 48–58. https://doi.org/10.1002/bit.27945.

Junker, B.H., 2004. Scale-Up Methodologies for Escherichia coli and Yeast Fermentation Processes. J. Biosci. Bioeng. 97 (6), 347–364. https://doi.org/10.1263/jbb.97.347.

Kaiser, S.C., Eibl, R., Eibl, D., 2011. Engineering characteristics of a single-use stirred bioreactor at bench-scale: The Mobius Cell Ready 3L bioreactor as a case study. Eng. Life Sci. 11 (4), 359–368. https://doi.org/10.1002/elsc.201000171.

Kaiser, S.C., Werner, S., Jossen, V., Kraume, M., Eibl, D., 2017. Development of a method for reliable power input measurements in conventional and single-use stirred bioreactors at laboratory scale. Eng. Life Sci. 17 (5), 500–511. https://doi.org/10.1002/elsc.201600096.

Langheinrich, C., Nienow, A.W., 1999. Control of pH in large-scale, free suspension animal cell bioreactors: Alkali addition and pH excursions. Biotechnol. Bioeng. 66 (3), 171–179. https://doi.org/10.1002/(SICI)1097-0290(1999)66:3<171::AID-BIT5>3.0.CO;2-T.

Lopes, A.G., 2015. Single-use in the biopharmaceutical industry: a review of current technology impact, challenges and limitations. Food Bioproducts Processing Inst. Chem. Eng. 93 (November), 98–114. https://doi.org/10.1016/j.fbp.2013.12.002.

Lu, R.-M., Hwang, Y.-C., Liu, I.-J., Lee, C.-C., Tsai, H.-Z., Li, H.-J., Wu, H.-C., 2020. Development of therapeutic antibodies for the treatment of diseases. J. Biomed. Sci. J. Biomed. Sci. 27 (1). https://doi.org/10.1186/s12929-019-0592-z.

Melton, L.A. et al., 2010. Dismt - Determination of mixing time through color changes, 6445. doi: 10.1080/00986440212077.

Micheletti, M., Barrett, T., Doig, S.D., Baganz, F., Levy, M.S., Woodley, J.M., Lye, G.J., 2006. Fluid mixing in shaken bioreactors: Implications for scale-up predictions from microlitre-scale microbial and mammalian cell cultures. Chem. Eng. Sci. 61 (9), 2939–2949. https://doi.org/10.1016/j.ces.2005.11.028.

Mitchell, E.T., Myers, K.J., Janz, E.E., Fasano, J.B., 2008. Solids suspension agitation in square tanks. Can. J. Chem. Eng. 86 (1), 110–116. https://doi.org/10.1002/cjce.20004.

Mollet, M. et al., 2004. Bioprocess Equipment : Characterization of Energy Dissipation Rate and Its Potential to Damage Cells.

Narayanan, H., Sponchioni, M., Morbidelli, M., 2022. Integration and digitalization in the manufacturing of therapeutic proteins. Chem. Eng. Sci. 248 (117159), 1–24. https://doi.org/10.1016/j.ces.2021.117159.

Nienow, A.W., 1997. On impeller circulation and mixing effectiveness in the turbulent flow regime. Chem. Eng. Sci. 52 (15), 2557–2565. https://doi.org/10.1016/S0009-2509(97)00072-9.

Nienow, A.W., 2006. Reactor engineering in large scale animal cell culture. Cytotechnology 50 (1–3), 9–33. https://doi.org/10.1007/s10616-006-9005-8.

Nienow, A.W., 2014. Stirring and stirred-tank reactors. Chem.-Ing.-Tech. 86 (12), 2063–2074. https://doi.org/10.1002/cite.201400087.

Nienow, A.W., 2021. The impact of fluid dynamic stress in stirred bioreactors – the scale of the biological entity: a personal view. Chem.-Ing.-Tech. 93 (1–2), 17–30. https://doi.org/10.1002/cite.202000176.

Nienow, A.W., Scott, W.H., Hewitt, C.J., Thomas, C.R., Lewis, G., Amanullah, A., Kiss, R., Meier, S.J., 2013a. Scale-down studies for assessing the impact of different stress parameters on growth and product quality during animal cell culture. Chem. Eng. Res. Des. Inst. Chem. Eng. 91 (11), 2265–2274. https://doi.org/10.1016/j.cherd.2013.04.002.

Nienow, A.W., Rielly, C.D., Brosnan, K., Bargh, N., Lee, K., Coopman, K., Hewitt, C.J., 2013b. The physical characterisation of a microscale parallel bioreactor platform with an industrial CHO cell line expressing an IgG4. Biochem. Eng. J. Elsevier B.V. 76, 25–36. https://doi.org/10.1016/j.bej.2013.04.011.

Nienow, A.W., Isailovic, B., Barrett, T.A., 2016. Design and Performance of Single-Use, Stirred-Tank Bioreactors. Bioprocess Int. 14 (10), 12–21 https://bioprocessintl.com/2016/design-performance-single-use-stirred-tank-bioreactors/.

Osman, J.J., Birch, J., Varley, J., 2002. The response of GS-NS0 myeloma cells to single and multiple pH perturbations. Biotechnol. Bioeng. 79 (4), 398–407. https://doi.org/10.1002/bit.10198.

Paul, K., Herwig, C., 2020. Scale-down simulators for mammalian cell culture as tools to access the impact of inhomogeneities occurring in large-scale bioreactors. Eng. Life Sci. 20 (5–6), 197–204. https://doi.org/10.1002/elsc.201900162.

Raffel, M. et al., 2018. Particle image velocimetry: a practical guide. In: Particle Image Velocimetry: A Practical Guide, pp. 1–32. doi: 10.1007/978-3-319-68852-7_1.

Restelli, V. et al., 2006. The effect of dissolved oxygen on the production and the glyocsylation profile of recombinant human erythropoietin produced from CHO cells. Biotechnol. Bioeng. 94 (3), 481–494. https://doi.org/10.1002/bit.20875.

Rodriguez, G., Anderlei, T., Micheletti, M., Yianneskis, M., Ducci, A., 2014. On the measurement and scaling of mixing time in orbitally shaken bioreactors. Biochem. Eng. J. Elsevier B.V. 82, 10–21. https://doi.org/10.1016/j.bej.2013.10.021.

Rotondi, M., Grace, N., Betts, J., Bargh, N., Costariol, E., Zoro, B., Hewitt, C.J., Nienow, A.W., Rafiq, Q.A., 2021. Design and development of a new ambr250® bioreactor vessel for improved cell and gene therapy applications. Biotechnol. Lett. Springer, Netherlands 43 (5), 1103–1116. https://doi.org/10.1007/s10529-021-03076-3.

Samaras, J.J., Ducci, A., Micheletti, M., 2020. Flow, suspension and mixing dynamics in DASGIP bioreactors, Part 2. AIChE J 66 (11), 1–15. https://doi.org/10.1002/aic.16999.

Samaras, J.J., Micheletti, M., Ding, W., 2022. Transformation of biopharmaceutical manufacturing through single-use technologies: current state, remaining challenges, and future development. Annu. Rev. Chem. Biomol. Eng. 13, 73–97. https://doi.org/10.1146/annurev-chembioeng-092220-030223.

Schirmer, C., et al., 2020. How to Produce mAbs in a Cube-Shaped Stirred Single-Use Bioreact. Available from: <http://www.springer.com/series/7651>.

Schirmer, C., Maschke, R.W., Pörtner, R., Eibl, D., 2021. An overview of drive systems and sealing types in stirred bioreactors used in biotechnological processes. Appl. Microbiol. Biotechnol. 105 (6), 2225–2242. https://doi.org/10.1007/s00253-021-11180-7.

Sewell, D.J., Turner, R., Field, R., Holmes, W., Pradhan, R., Spencer, C., Oliver, S.G., Slater, N.KH., Dikicioglu, D., 2019. Enhancing the functionality of a microscale bioreactor system as an industrial process development tool for mammalian perfusion culture. Biotechnol. Bioeng. John Wiley & Sons Ltd 116 (6), 1315–1325. https://doi.org/10.1002/bit.26946.

Simmons, M.J.H., Zhu, H., Bujalski, W., Hewitt, C.J., Nienow, A.W., 2007. Mixing in a model bioreactor using agitators with a high solidity ratio and deep blades. Chem. Eng. Res. Des. 85 (5), 551–559. https://doi.org/10.1205/cherd06157.

Stettler, M., Zhang, X., Hacker, D.L., DeJesus, M., Wurm, F.M., 2007. Novel orbital shake bioreactors for transient production of CHO derived IgGs. Biotechnol. Prog. 23 (6), 1340–1346. https://doi.org/10.1021/bp070219i.

Tajsoleiman, T., Mears, L., Krühne, U., Gernaey, K.V., Cornelissen, S., 2019. An industrial perspective on scale-down challenges using miniaturized bioreactors. Trends Biotechnol. Elsevier Ltd 37 (7), 697–706. https://doi.org/10.1016/j.tibtech.2019.01.002.

Teworte, S., Malcı, K., Walls, L.E., Halim, M., Rios-Solis, L., 2022. Recent advances in fed-batch microscale bioreactor design. Biotechnol. Adv. Elsevier Inc Biotechnology Advances 55, 107888. https://doi.org/10.1016/j.biotechadv.2021.107888.

Thielicke, W., Sonntag, R., 2021. Particle image velocimetry for MATLAB: accuracy and enhanced algorithms in PIVlab. J. Open Res. Software 9, 1–14. https://doi.org/10.5334/JORS.334.

Velez-Suberbie, M.L., Betts, J.P.J., Walker, K.L., Robinson, C., Zoro, B., Keshavarz-Moore, E., 2018. High throughput automated microbial bioreactor system used for clone selection and rapid scale-down process optimization. Biotechnol. Prog. 34 (1), 58–68. https://doi.org/10.1002/btpr.2534.

Wyrobnik, T.A., et al., 2022. In: Engineering characterization of the novel Bach impeller for bioprocessing applications requiring low power inputs', Chemical Engineering Science, 252. Elsevier Ltd, p. 117263. https://doi.org/10.1016/j.ces.2021.117263.

Xing, Z., Kenty, B.M., Li, Z.J., Lee, S.S., 2009. Scale-up analysis for a CHO cell culture process in large-scale bioreactors. Biotechnol. Bioeng. 103 (4), 733–746. https://doi.org/10.1002/bit.22287.

Zhu, H., Nienow, A.W., Bujalski, W., Simmons, M.J.H., 2009. Mixing studies in a model aerated bioreactor equipped with an up- or a down-pumping "Elephant Ear" agitator: power, hold-up and aerated flow field measurements. Chem. Eng. Res. Des. 87 (3), 307–317. https://doi.org/10.1016/j.cherd.2008.08.013.